DEM Investigation of Sliding Mechanisms in a 3D-Printed Flat Arch

Antonino Iannuzzo[1(✉)], Michele Lanza[2], Lino Cusano[3], Francesco Picariello[4], and Giuseppe Maddaloni[1]

[1] Department of Engineering, University of Sannio, Piazza Roma, 28, 82100 Benevento, Italy
{aniannuzzo,maddaloni}@unisannio.it
[2] Tecnica y Proyectos S.A., Madrid, Spain
mlanza@typsa.es
[3] University of Sannio, Benevento, Italy
l.cusano@studenti.unisannio.it
[4] Universitas Mercatorum, Rome, Italy
francesco.picariello@unimercatorum.it

Abstract. This paper presents a preliminary experimental and numerical investigation of the mechanical response of a flat arch using a 3D-printed small-scale physical model analysed through distinct element modelling. Based on the historical rules introduced by Coulomb, the arch is designed with joint inclinations chosen to guarantee a controlled minimum friction capacity, and fabricated via fused filament fabrication. Due to the characteristically high horizontal thrust, flat arches typically experience small abutment displacements and settle into a minimum thrust configuration. Two experimental tests with different interface properties are performed to investigate this mechanical response under increasing horizontal displacement. The in-house VEDEM+ plugin is adopted to link CAD modelling with 3DEC (Itasca), enabling precise geometric modelling and systematic post-processing of the structural response. A parametric study is subsequently carried out to interpret the experimental observations. The results demonstrate that interface friction significantly affects both the displacement capacity and the governing collapse mechanism. In particular, as expected, in a high-friction scenario, sliding is avoided, and a pure hinging mechanism governs collapse from the outset. Conversely, when friction capacity is low, sliding initiates at the interfaces and persists until the internal thrust finds a configuration in which the force inclination at each joint falls within the friction cone; once this condition is met, a hinging mechanism develops and ultimately governs collapse.

Keywords: Masonry structures · Flat arch · 3DEC · Displacement capacity · Distinct element modelling · Rigid blocks · Experimental tests

© The Author(s), under exclusive license to Springer Nature Switzerland AG 2027
O. Gervasi et al. (Eds.): ICCSA 2026 Workshops, LNCS 16758, pp. 446–463, 2027.
https://doi.org/10.1007/978-3-032-30497-1_27

1 Introduction

Traditional masonry is an uncommon material in contemporary construction, feeling largely unfamiliar in the 21st century, even though most of our built cultural heritage is composed of masonry constructions. Unlike modern structural materials, it does not conform to standard assumptions such as homogeneity, isotropy, or elastic behaviour characterised by parameters like Young's modulus and Poisson's ratio. While masonry performs well under compression, it is extremely weak in tension, exhibiting a unilateral behaviour that is crucial to understanding its structural performance [28,32]. Historic masonry structures, furthermore, frequently contain cracks, which demand an analytical approach fundamentally different from that developed for modern engineering materials such as steel and reinforced concrete. Such an approach was widely adopted, even in the absence of rigorous mathematical foundations, particularly through graphic statics during the 18th and 19th centuries. A key insight underpinning this approach came from Robert Hooke (1675) [29], who was the first to accurately analyse the behaviour of masonry arches by drawing an analogy with the well-known geometry of a hanging chain [4]. Hooke did not derive the mathematical equation of the catenary curve; his fundamental contribution was instead the recognition of the structural similarity between these two seemingly different systems. A few decades later, the mathematician Gregory (1697) [33] refined this idea by asserting that the catenary is the true form of an arch, and that if arches of other shapes remain standing, it is because a catenary can be found lying within their thickness. Notable examples include the assessment of the dome of St. Peter's Basilica by Poleni [52], while the earlier report by *I tre Mattematici*, that is Le Seur, Jacquier, and Boscovich [37], made pioneering use of the virtual work principle. In 1807, Thomas Young [59] similarly applied hanging models to demonstrate the behaviour of masonry bridges. The same principle guided the design of new structures, as demonstrated by Antoni Gaudí in his work on the Sagrada Família in Barcelona. For a broader overview of the use of these models in architectural design, Graefe [27] provides an extended review. It was Heyman who, from the 1960s onwards, successfully framed this long-standing practice within the rigorous framework of modern Limit Analysis, providing it with a consistent mathematical foundation and significantly advancing the understanding of masonry architecture [28]. This was achieved through three fundamental assumptions: no tensile strength, infinite compressive resistance, and no sliding failure. Modern applications of graphic static analyses through line of thrust in 2D and 3D geometries can be found in [3,12,13,23,43,57,58]

A masonry structure consists of stones assembled in a specific arrangement, with or without mortar, to achieve a particular geometric form that allows internal forces to be transmitted to the foundations through purely compressive paths, consistent with the material constraints of negligible tensile strength and sliding capacity. The no-sliding assumption is required to apply standard Limit Analysis to no-tension materials and is generally considered satisfied either by the confining effect of high compressive stresses, by geometric interlocking between blocks, or by a combination of both, though it should in principle be

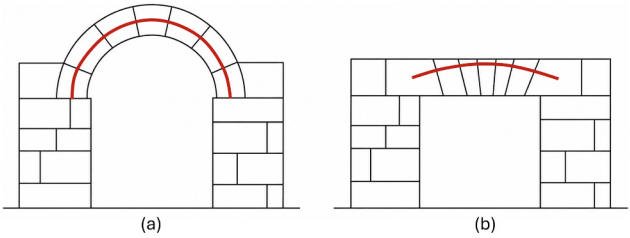

Fig. 1. Forces (in red) acting on the abutments of a semicircular arch and a flat arch of equal span under self-weight (redrawn from [16]). (Color figure online)

verified a posteriori. For more information, the reader is also referred to [1] and references therein. As will be shown in the present work, this assumption is not always satisfied experimentally: numerical analyses capture this behaviour effectively, revealing that sliding mechanisms can occur as long as the hinging mechanism is energetically preferred, that is, as long as the ratio between tangential and normal forces remains within a Mohr-Coulomb-type sliding criterion. This is further confirmed by Distinct Element Analysis simulations.

1.1 The Stone Lintel Arch

The stone lintel arch, composed of wedge-shaped voussoirs, can be seen as the flattest variation of the more common semi-circular arch (Fig. 1). Heyman demonstrated that, under ideal conditions-where there is no slipping between adjacent voussoirs and the abutments remain sufficiently rigid-the lintel arch remains stable regardless of the load [28]. However, due to its shape, it generates greater horizontal forces than an equivalent semi-circular arch with the same span. This increases the likelihood of abutment yielding, which may eventually lead to structural failure, as illustrated in Fig. 2, where two collapse mechanisms are shown: hinging and sliding. In this paper, it will be shown how both mechanisms can be predicted by considering the forces acting on the block interfaces, and how the structural response transitions from sliding to hinging once the frictional capacity is mobilised. A monolithic lintel (Fig. 3) subjected to loading behaves similarly to a flat arch once it cracks at the centre, maintaining stability as long as the abutments remain rigid [31]. Cutting a lintel into voussoirs offers a practical advantage: it preempts uncontrolled cracking, avoids unsightly fractures, and produces a more predictable structural system. This behaviour is readily understood by considering the fixed-ended beam of Fig. 4, composed of a material weak in tension such as stone or concrete: the flexural capacity is first exploited, and once cracks appear, the element responds as a flat arch composed of discrete blocks. In this sense, pre-cutting the lintel into voussoirs is preferable, as it allows the designer to control where openings between blocks will form.

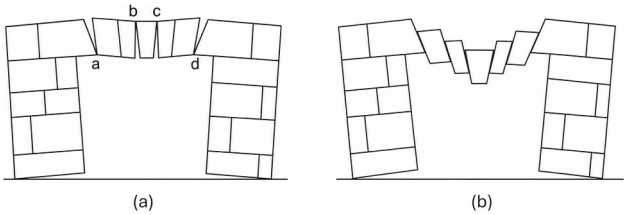

Fig. 2. Structural response of a lintel arch to abutment movement: (a) hinging mechanism with non-critical hinges forming at points a, b, c, and d; (b) sliding-dominated mechanism due to support displacement causes the voussoirs to shift relative to each other (redrawn from [16]).

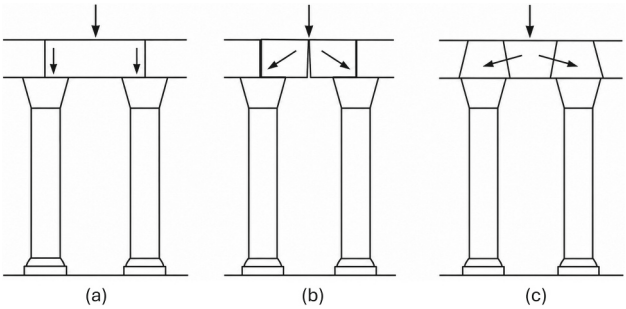

Fig. 3. The structural response of a monolithic lintel: (a) functioning as a beam, (b) transitioning into a simple lintel arch upon cracking, and (c) comparison with a traditional lintel arch (redrawn from [16]).

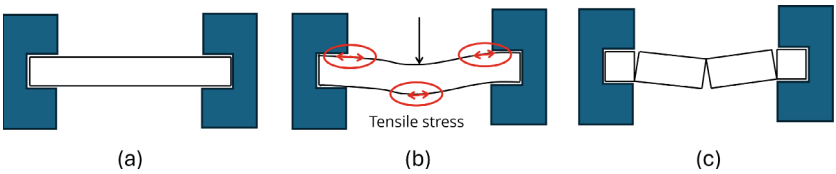

Fig. 4. Structural behaviour of a fixed-ended beam made up of material weak in tension.

1.2 Brief Historical Background

Although the flat arch was present in Near Eastern mud-brick architecture as early as the second millennium BC, it does not appear to have been widely adopted into Greek architecture alongside the semicircular voussoir arch in the late fourth century BC, remaining uncommon throughout the Hellenistic period [5]. This is likely because the Greeks primarily used the semicircular arch as a decorative element rather than out of structural necessity, as most openings could be spanned with a simple lintel. The availability of strong limestone

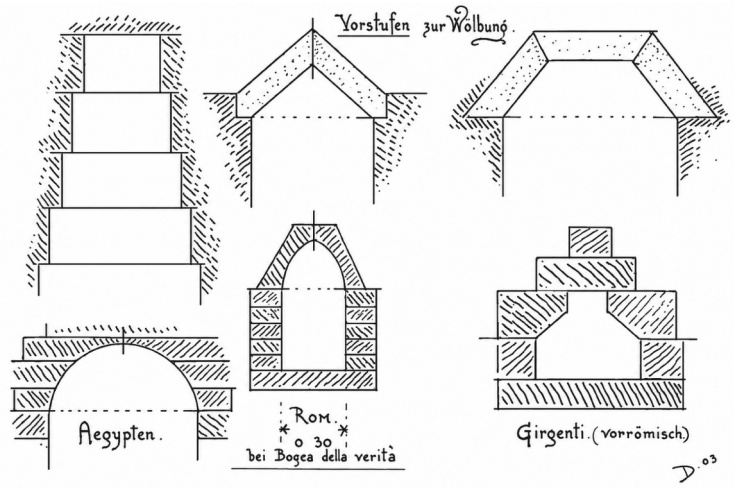

Fig. 5. Historical evolution of arch forms across ancient cultures: corbelled construction (Egypt), pointed arch (Rome, near the Bocca della Verità), and pre-Roman flat arch configurations (Girgenti), illustrating the progressive transition from corbelling to true voussoir arches *Vorstufen zur Wölbung* (from [16]).

and marble in Greece favoured the continued use of stone lintels in monumental construction, reflecting a generally conservative approach to material choice.

The standard maximum span for stone lintels in Greek stoae [8] and most Greek temples [18] was around 3.0–3.5 m, keeping tensile forces well below the theoretical strength of the stone. For wider openings, various reinforcement techniques were employed [9,19], or wooden lintels were used where considered aes-

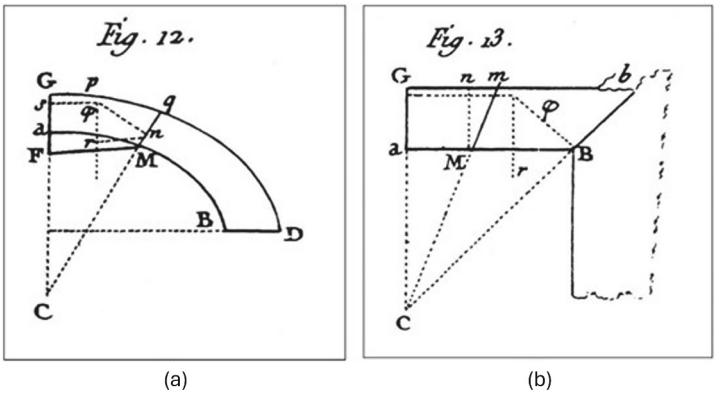

Fig. 6. Coulomb's study of joint inclination for a vault in equilibrium without friction: (a) general case; (b) application to a plate-bande [7].

thetically acceptable [8]. The transition from corbelling to the direct placement of stones against one another marked an important evolution in construction technique. Initially, two stones were positioned this way, then three, and from this arrangement the development of the true keystone vault was only a small step away (Fig. 5). Mycenaean architecture came to an end in the 11th century BC, giving way to a second pre-Hellenic period during the Iron Age, influenced by Assyrian and Egyptian elements and flourishing in Asia Minor under Alyattes and Croesus. This tradition encompassed the Lycian and Lydian kingdoms, the Ionian coast, the Aegean islands, and Etruria, with a common cultural influence stretching from the Persian Gulf to Tuscany. Three key developments characterised this era: the introduction of the alphabet, the invention of coinage, and the adoption of iron tools in craftsmanship and construction. During the Medieval period, flat arches played a secondary role to the pointed arches dominant in Gothic architecture, serving structural and decorative purposes in doorways, windows, and stained-glass tracery, as well as in bridge construction for short spans. In the Renaissance, a revival of classical ideals restored flat arches to prominence, making them key features in facades, arcades, and porticoes, often adorned with detailed mouldings and keystones, as seen in the work of Andrea Palladio. In the Baroque period, flat arches became increasingly elaborate, emphasising ornamentation over structural function, with sculptural details enriching facades, entrances, and windows. In the contemporary period, flat arches have experienced a resurgence thanks to modern materials such as reinforced concrete and steel, appearing in minimalist and modernist designs, bridges, urban infrastructure, and adaptive reuse projects, where their ability to span greater distances and their aesthetic versatility make them a functional and innovative element.

2 Methodology

This section outlines the methodology adopted in the present work: physical tests on a small-scale flat arch are performed and the corresponding results interpreted through the Distinct Element Method (DEM) software 3DEC by Itasca [35].

2.1 Design and Physical Testing of a 3D-Printed Flat Arch

The proportions of plate-bandes, defined as the ratio between thickness t and span s, generally range from 1/4 to 1/3 in stockier configurations, while the most slender examples exhibit ratios below 1/20. During the 15th century, a common ratio was approximately 1/8, adhering to a simple geometric principle: the centre forms an equilateral triangle with the intrados, and the plate-bande should encompass an arc of a circle. The joints are typically flat, though in some instances they feature a rebated or stepped profile, and the wedge shape of the voussoirs produces acute angles at the stone corners, which may result in localised fractures. De La Hire observed that when an arch or barrel vault collapses, it typically fractures at a point between the keystone and the springing,

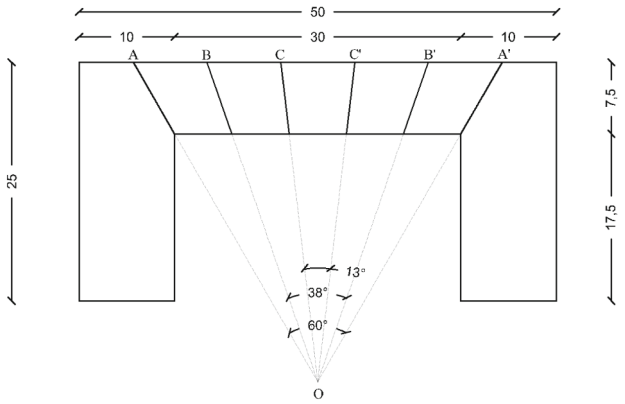

Fig. 7. Stereotomy of the flat arch designed according to [7], showing joint inclinations and main dimensions in mm.

known as the joint of rupture, and theorised that the thrust at this point must be tangent to the intrados curve. Couplet subsequently adopted the no-sliding hypothesis, analysing the equilibrium of the plate-bande under the assumption of zero friction between voussoirs. Coulomb imposed two conditions: forces must act perpendicular to the joints and must remain within the masonry, arriving at the same conclusion as Couplet: all joints must converge toward a common centre (Fig. 6). For further remarks on the collapse of masonry arches with Coulomb friction, the reader is referred to [56]. The stereotomy of the flat arch was thus defined according to the rule of converging joints proposed by Coulomb (Fig. 7) considering five voussoirs and two abutment blocks.

To investigate the structural behaviour of the flat arch experimentally, a scaled model was produced using the Bambu Lab X1-Carbon filament-based 3D printer (Fig. 8a). The model was fabricated in PLA, a biodegradable bioplastic



(a) (b)

Fig. 8. (a) 3D-printed modular flat arch consisting of hollow voussoirs with removable caps to allow filling blocks to increase material density; (b) experimental setup of the flat arch specimen.

widely used in additive manufacturing and well-suited for producing accurate and repeatable prototypes. As shown in Fig. 8a, a hollow geometry was adopted for the blocks to allow internal filling with the desired material to increase the material density; each block features a wall thickness of 3 mm and a removable top cap to enable filling, sealing, and mass control before testing. The 3D-printed specimen is shown in Fig. 8b; notably, the arch remains stable even at low friction values.

2.2 3DEC Parametric Investigation Through VEDEM+ Plugin

Parametric numerical analyses were performed using 3DEC 9.0 by Itasca [35] as distinct element modelling (DEM) solvers, widely used in current engineering applications [46,47,55]. Different block-based approaches were developed in recent years, starting from the work of [25,26,38,53] until recent ones [20,30,34,44,45,47–51,54] 3DEC was selected for three reasons: i) its three-dimensional formulation for capturing the structural response; ii) the possibility of selecting different material properties that can be used to match the physical characteristics of real and 3D-printed specimens; iii) and the opportunity of extracting features and developing custom post-processing routines.

Two principal strategies can be used in 3DEC to model blocks based on how their rigidity and internal deformation are handled. **Perfectly rigid elements** treat each block as a rigid body with six degrees of freedom. All forces acting on the block are reduced to the centroid, generating resultant force and moment vectors; the equations of motion directly yield translational and rotational accelerations at each time step. In 3DEC, a rigid block is represented as a convex polyhedron. This formulation requires minimal material property input (only joint parameters), is computationally efficient for explicit time-stepping, and

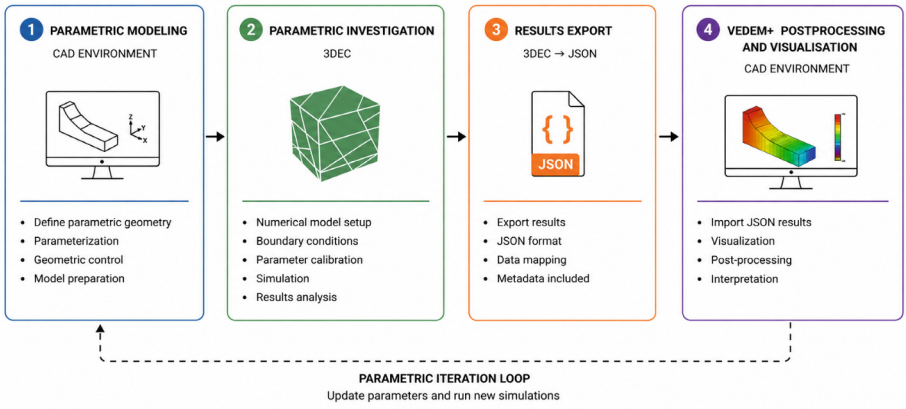

Fig. 9. VEDEM+ pipeline [14] used to assess the mechanical response of a flat arch: from the geometry definition, going through the 3DEC analyses and the visualisation of the post-processed results.

is physically accurate whenever the joint compliance vastly exceeds the block compliance, as is the case for strong stone masonry or hard 3D-printed blocks. **Deformable blocks** are modelled by subdividing each polyhedral block into an internal mesh of tetrahedral FE with uniform-strain [11]. Nodal translations are the kinematic unknowns and the corresponding associated mass is determined from the associated Voronoi cell. The equations of motion are applied to translational accelerations of the nodes, allowing the evaluation of internal stress distributions.

Contact representation and constitutive models in 3DEC are modelled using the point contact approach [36]. For polyhedral blocks in three dimensions, the contact between two faces can involve any combination of vertex, edge, and face interactions. [10]. 3DEC efficiently handles the contact using the *common plane* concept. Once two blocks are identified as being in contact, 3DEC defines specific *sub-contacts*, i.e. the actual point contacts, based on the geometry of the interaction. The mechanical behaviour at each sub-contact is governed by a joint constitutive model. In the present research, the *Mohr-Coulomb* model was adopted using only the joint normal and shear stiffness values as mechanical parameters. These are the most sensitive parameters in a 3DEC model. Their values can be defined through direct measurements or by modelling the joint compliance, treating the joint assembly as a continuum [40]. These values can also be reduced to speed up the calculation, but preliminary parametric analyses are needed [17,40]. It is worth pointing out that, because of the unilateral behaviour, contact forces exist only if a small elastic interpenetration between blocks is present. The elastic phase of the contact response is governed by the following relation between the increment in normal stress and the increment in normal interpenetration:

$$\Delta\sigma_n = k_n \, \Delta u_n \tag{1}$$

Contact stiffness is therefore a critical parameter: an excessively low normal stiffness leads to unrealistic block interpenetration and must be calibrated with care. In the present work, the Mohr-Coulomb model with tension cut-off is adopted, requiring normal and shear stiffness, friction angle, cohesion, and tensile strength as input. Post-processing is performed in a CAD environment, where interface forces are extracted and examined to interpret the mechanical response of the flat arch. All 3DEC analyses were performed using the VEDEM+ (Visualisation Environment for Distinct Element Method) plugin [14]. VEDEM+ is a dedicated pipeline (Fig. 9) developed to integrate CAD modelling with 3DEC, extending its post-processing capabilities and enabling a meaningful interpretation of results, following a strategy similar to that adopted in [17]. Specifically, VEDEM+ allows the visualisation of interface forces, internal stress diagrams, force comparisons across loading or displacement sequences, and contact pressure distributions, providing a comprehensive picture of force transmission within the structure. For further details, the reader is referred to [14].

3 Physical Testings: Results

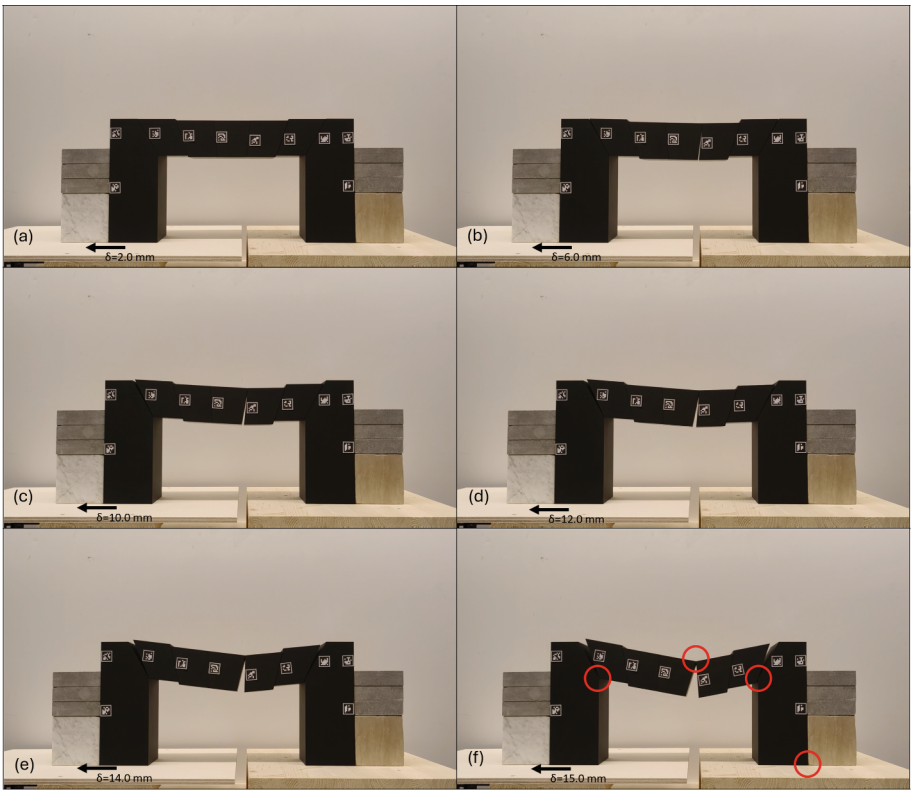

Fig. 10. Experimental displacement capacity analysis of the low-friction flat arch. Specifically, deformations and joint openings are observed for 2.0 mm (a), 6.0 mm (b), 10.0 mm (c), 12.0 mm (d), 14.0 mm (e), and the formation of the four-hinge collapse mechanism at 15.0 mm (f), where the active hinges are highlighted in red. (Color figure online)

The experimental campaign on the 3D-printed flat arch model is presented in this section. A dedicated test apparatus was assembled, incorporating a linear actuator designed to apply a controlled lateral outward displacement to the left abutment, to activate the collapse mechanisms typical of flat arch behaviour. This applied displacement was selected to force the arch into a minimum thrust condition, which is the standard condition of a flat arch. Indeed, external settlements activate different internal thrust conditions. For more information and novel computational, experimental and theoretical approaches, the reader is referred to [2,21,22,24,39,41,42]. The test followed a step-by-step procedure: the voussoirs and abutment blocks were first filled with sand to increase their

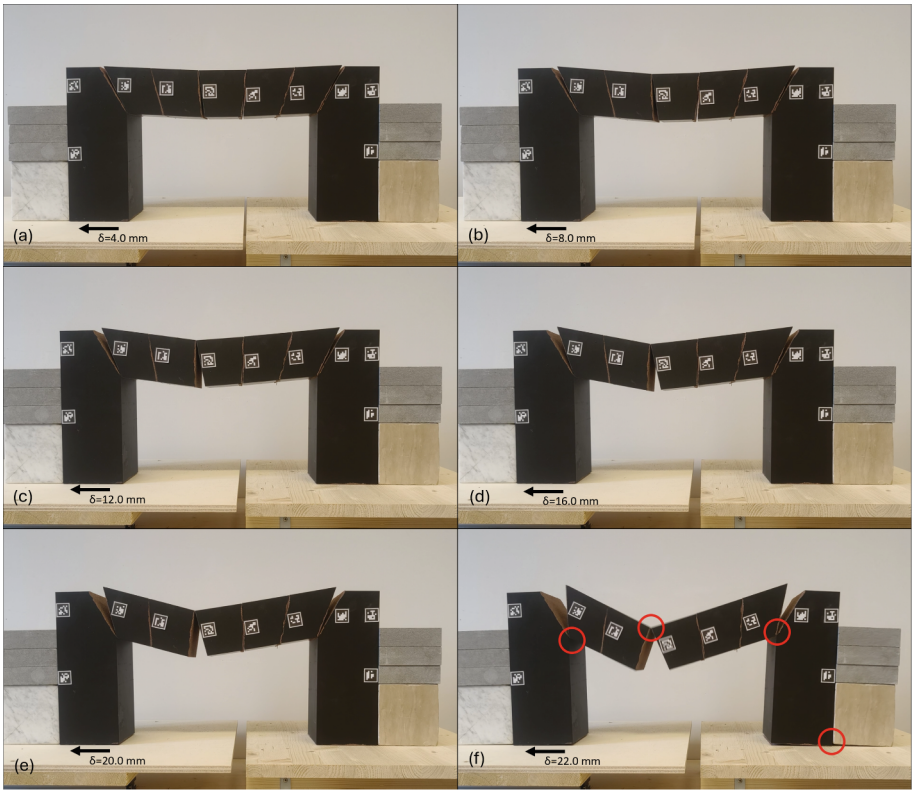

Fig. 11. Displacement capacity analysis of the flat arch having interfaces with friction $\phi = 35°$ due to the application of a layer of dust sand. Deformation and hinge formation for 4.0 mm (a), 8.0 mm (b), 12.0 mm (c), 16.0 mm (d), 20.0 mm (e), and the activation of the four-hinge (red circles) collapse mechanism at 22.0 mm (f). (Color figure online)

mass, then sealed in preparation for loading. The voussoirs were equipped with QR codes to monitor displacements during testing, following the approach developed in [15]; these results will be presented and discussed in a forthcoming publication. Friction coefficients were determined through static inclined plane tests and are reported in Table 2. Two friction conditions were considered. The first corresponds to a low-friction scenario based on the properties of PLA: the static friction coefficient of PLA ranges between 0.04 and 0.2 [6], and the wood-PLA interface friction angle was experimentally found to be approximately 17°. To prevent premature sliding at the abutment base under this low-friction condition, external blocks were placed adjacent to the buttresses. The friction angle for PLA-to-PLA contact was determined from laboratory tests and converged on approximately 13°. In the second configuration, a layer of sand was introduced at the block interfaces and beneath the flat arch buttresses, providing an effective friction angle of approximately 35° as determined from inclined plane

Table 1. Density of the elements.

Element	A	D	C	B	Flat Arch
ρ [kg/m^3]	2500	2700	2600	1716	1716

Table 2. Contacts friction angles [°] - letters are indicated in Fig. 12, while FA denotes the friction angles among flat arch elements, including the two buttresses.

Contact	S-A	S-D	S-B	A-C	D-C	FA-FA
Case 1	20	20	17	15	15	13
Case 2	20	20	25	15	15	35

tests. The results for both friction conditions are reported in Figs. 10 and 11. A comparison between the two tests reveals distinct mechanical behaviours. In the first test, with unfixed abutments and a uniform low PLA-to-PLA friction angle, collapse occurred at a displacement of approximately 15 mm. As shown in Fig. 10, sliding of the three central voussoirs is observed from the very onset of loading. At approximately 6 mm of displacement, the response transitions to a hinging-dominated mechanism, accompanied by an increase in horizontal thrust. Beyond 10 mm, hinging becomes the governing mechanism, causing local sliding at the base of the external abutments and buttresses as well as counter-rotation of the lateral blocks placed to restrain the external abutments (Fig. 10e). Collapse occurs via a four-hinge mechanism at approximately 15 mm (Fig. 10f). In the second test (Fig. 11), the increased friction angle of 35° due to the sand layer produced a markedly different response: no sliding was observed and a pure hinging mechanism developed, allowing the structure to sustain larger displacements.

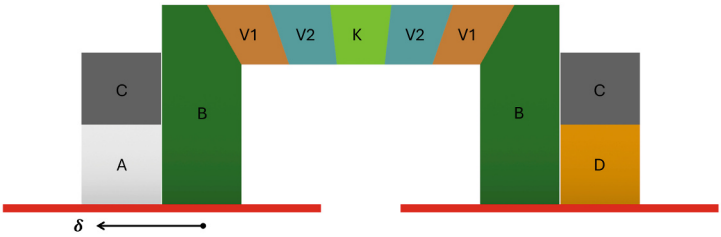

Fig. 12. 3DEC digital model: geometry discretisation. The two red blocks are considered supports. The material parameters are reported in Table 1 and 2. Between blocks B and C-A and C-D, there is a numerical gap to better model the small detachment noted in the physical test. (Color figure online)

4 3DEC Parametric Investigation

A parametric study in 3DEC was conducted to investigate the flat arch response under varying interface friction, improving model fidelity to the physical conditions observed experimentally. The geometry of the numerical model is shown in Fig. 12, including the flat arch voussoirs and the external marble support elements. The two abutment blocks (shown in red) are treated as supports; only the left one is subjected to an imposed foundation displacement, consistent with the experimental setup. Block densities and friction coefficients are reported in Tables 1 and 2, respectively, with friction values taken directly from the experimental measurements. Two analyses are performed, corresponding to the low- and high-friction conditions tested in the laboratory.

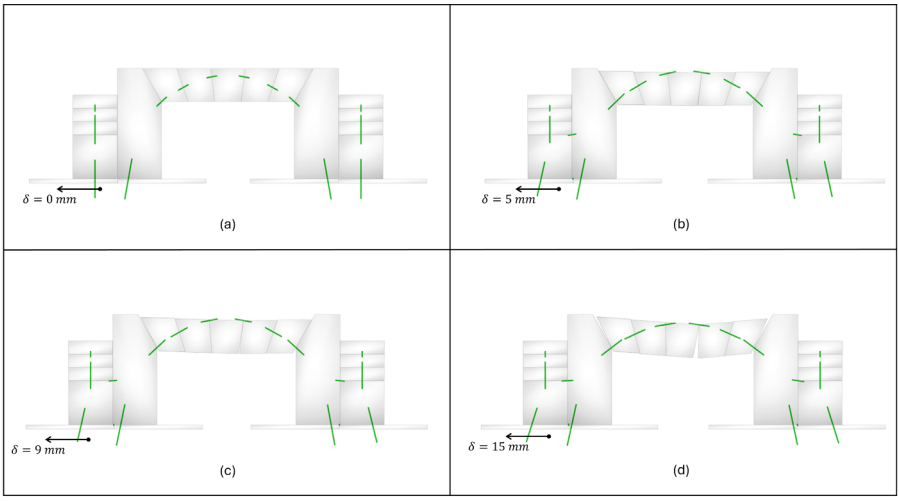

Fig. 13. VEDEM+ visualisation of interface resultants considering $\phi = 13°$ (case 1 of Table 2): the flat arch initially exhibits a sliding mechanism, which transitions to hinging until collapse, where sliding reappears between the left abutment and buttress and the moving support due to the high horizontal thrust induced by the three-hinge mechanism.

The right abutment was fixed, while a controlled displacement was applied to the left abutment following the same loading protocol as in the experimental tests. Custom scripts were developed in 3DEC to automate geometry import and to drive the displacement-controlled analysis through to collapse. Displacement steps were imposed as velocity inputs at the left abutment, with equilibrium verified after each step. The results of the two analyses are reported in Figs. 13 and 14.

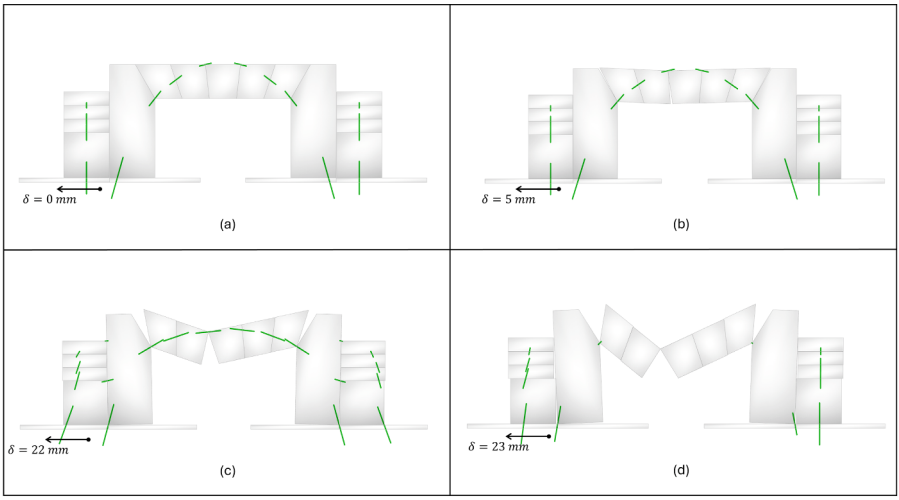

Fig. 14. VEDEM+ visualisation of resultants assuming $\phi = 35°$ (case 2 of Table 2): the arch shows a typical three-hinge mechanism until the collapse, where a fourth hinge forms at the base.

5 Conclusions

This paper has presented a preliminary experimental and numerical investigation of the mechanical response of a flat arch, designed according to Coulomb's converging-joint rule and fabricated via fused filament fabrication using a 3D-printed scaled model. Two experimental tests with different interface friction conditions were conducted by imposing a controlled horizontal displacement at one abutment, replicating the minimum thrust configuration characteristic of flat arches under service conditions.

The VEDEM+ plugin [14] was adopted to link CAD modelling with 3DEC (Itasca) analyses, enabling precise geometric modelling and detailed post-processing throughout the loading sequence. A parametric study was subsequently carried out to complement and interpret the experimental observations. The DEM analyses are in excellent agreement with the experimental results, confirming the reliability of the modelling approach. The following conclusions can be drawn:

- interface friction significantly affects both the displacement capacity and the governing collapse mechanism;
- when friction is sufficient, sliding is suppressed and a pure hinging mechanism governs collapse from the outset;
- when friction capacity is low, sliding initiates at the interfaces and persists until the ratio between shear and normal force at each joint falls within the friction cone; once this condition is met, hinging develops and ultimately governs collapse;

– in both cases, collapse is driven by the horizontal thrust, which increases monotonically as the hinge configuration approaches the limit state.

The present research highlight the importance of accurately account for interface friction in the assessment of flat arches, and demonstrate the effectiveness of combining physical testing with DEM for the study of collapse mechanisms.

Acknowledgments. This research is funded by the Italian Ministry of University and Research through the Programme "Rita Levi Montalcini for Young Researchers" (FFO 2020). The authors gratefully acknowledge Itasca for providing the 3DEC software under the 'Educational Discount Agreement'.

References

1. Aita, D., Beatini, V., Caruso, H., Garavaglia, E., Sgambi, L.: Some remarks on non-standard plastic behaviour with coulomb's friction starting from an unconventional stone flat arch. Eng. Struct. **326**, 119539 (2025). https://doi.org/10.1016/j.engstruct.2024.119539
2. Angelillo, M., Iannuzzo, A., Montanino, A.: Discretised continuum approaches: from continuum to dis-continuum. In: Discrete Computational Mechanics of Masonry Structures, pp. 95–163. Springer (2023). https://doi.org/10.1007/978-3-031-32476-5_3
3. Avelino, R.M., Iannuzzo, A., Van Mele, T., Block, P.: Assessing the safety of vaulted masonry structures using thrust network analysis. Comput. Struct. **257**, 106647 (2021)https://doi.org/10.1016/j.compstruc.2021.106647
4. Block, P., DeJong, M., Ochsendorf, J.: As hangs the flexible line: equilibrium of masonry arches. Nexus Netw. J. **8**(2), 13–24 (2006). https://doi.org/10.1007/s00004-006-0015-9
5. Boyd, T.D.: The arch and the vault in greek architecture. Am. J. Archaeol. **82**(1), 83–100 (1978)
6. Cardoso, P.H.M., de Oliveira, M.F.L., de Oliveira, M.G., da Silva Moreira Thiré, R.M.: 3d printed parts of polylactic acid reinforced with carbon black and alumina nanofillers for tribological applications. In: Macromolecular Symposia, vol. 394, p. 2000155. Wiley Online Library (2020)
7. Coulomb, C.A.: Essai sur une application des regles de maximis et minimis a quelques problemes de statique relatifs a l'architecture (essay on maximums and minimums of rules to some static problems relating to architecture (1973)
8. Coulton, J.J.: The architectural development of the greek stoa. (No Title) (1976)
9. Coulton, J., Murray, R.: Membrane associated components of the bacterial flagellar apparatus. Biochimica et Biophysica Acta (BBA)-Biomembranes **465**(2), 290–310 (1977)
10. Cundall, P.A.: Formulation of a three-dimensional distinct element model-part i. a scheme to detect and represent contacts in a system composed of many polyhedral blocks. In: International Journal of Rock Mechanics and Mining Siences & Geomechanics Abstracts, vol. 25, pp. 107–116. Elsevier (1988)
11. Cundall, P.A., Strack, O.: A discrete numerical model for granular assemblies. Géotechnique **29**(1), 47–65 (1979). https://doi.org/10.1680/geot.1979.29.1.47

12. Cusano, C., Angjeliu, G., Montanino, A., Zuccaro, G., Cennamo, C.: Considerations about the static response of masonry domes: A comparison between limit analysis and finite element method. Int. J. Masonry Res. Innov. **6**(4), 502–528 (2021). https://doi.org/10.1504/IJMRI.2021.118835
13. Cusano, C., Montanino, A., Olivieri, C., Paris, V., Cennamo, C.: Graphical and analytical quantitative comparison in the domes assessment: the case of san francesco di paola. Appl. Sci. **11**(8), 3622 (2021). https://doi.org/10.3390/app11083622
14. Cusano, L., Iannuzzo, A.: Vedem+: enhancing engineering assessment of complex stereotomic structures via 3dec-to-cad post-processing workflows. In: International Conference on Computational Science and Its Applications. Springer (2026)
15. Daponte, P., De Vito, L., Iannuzzo, A., Monaco, M., Neyestani, A., Picariello, F.: Low-cost marked tracking monitoring system for 3d-scaled masonry models. In: 2024 IEEE International Workshop on Metrology for Living Environment (MetroLivEnv), pp. 172–177. IEEE (2024)
16. DeLaine, J.: Structural experimentation: the lintel arch, corbel and tie in western roman architecture. World Archaeol. **21**(3), 407–424 (1990)
17. Dell'Endice, A., Iannuzzo, A., DeJong, M.J., Van Mele, T., Block, P.: Modelling imperfections in unreinforced masonry structures: Discrete element simulations and scale model experiments of a pavilion vault. Eng. Struct. **228**, 111499 (2021). https://doi.org/10.1016/j.engstruct.2020.111499
18. Dinsmoor, W.B.: The architecture of ancient Greece: an account of its historic development. Biblo & Tannen Publishers (1973)
19. Dorn, H.: A note on "structural antecedents of the i-beam". Technol. Cult. **9**(3), 415–418 (1968)
20. Fabbrocino, F., Olivieri, C., Luciano, R., Vaiano, G., Maddaloni, G., Iannuzzo, A.: Seismic performance of historic masonry buildings: a comparative analysis of equivalent frame and block-based methods. Alex. Eng. J. **109**, 359–375 (2024). https://doi.org/10.1016/j.aej.2024.08.043
21. Ferrero, C., Portioli, F.P., Calderini, C.: Lateral load response of a dry-joint masonry arch subject to vertical support displacements by rigid block analysis. Meccanica **60**(7), 2001–2018 (2025). https://doi.org/10.1007/s11012-024-01927-7
22. Galassi, S.: An alternative approach for limit analysis of masonry arches on moving supports in finite small displacements. Eng. Fail. Anal. **145**, 107004 (2023). https://doi.org/10.1016/j.engfailanal.2022.107004
23. Galassi, S., Tempesta, G.: Safety assessment of masonry undamaged and damaged arches subjected to gravitational loads and horizontal forces. a numeric procedure to identify the optimal thrust line. Int. J. Solids Struct. **301**, 112943 (2024). https://doi.org/10.1016/j.ijsolstr.2024.112943
24. Galassi, S., Zampieri, P.: A new automatic procedure for nonlinear analysis of masonry arches subjected to large support movements. Eng. Struct. **276**, 115359 (2023). https://doi.org/10.1016/j.engstruct.2022.115359
25. Gilbert, M., Casapulla, C., Ahmed, H.: Limit analysis of masonry block structures with non-associative frictional joints using linear programming. Comput. Struct. **84**(13–14), 873–887 (2006). https://doi.org/10.1016/j.compstruc.2006.02.005
26. Gilbert, M., Melbourne, C.: Rigid-block analysis of masonry structures. Struct. Eng. **72**(21) (1994)
27. Graefe, R.: Zur formgebung von bögen und gewölben. Architectura (1986)
28. Heyman, J.: The stone skeleton. Int. J. Solids Struct. **2**(2), 249–279 (1966). https://doi.org/10.1016/0020-7683(66)90018-7

29. Hooke, R.: A description of helioscopes and some other instruments. No. 3, TR (1974)
30. Hua, Y., Buzzetti, M., Pingaro, N., da Silva, L.C., Milani, G.: A computerized tool for the kinematic limit analysis of 2d masonry structures failing on a tilting table. SoftwareX **30**, 102180 (2025). https://doi.org/10.1016/j.softx.2025.102180
31. Huerta, S.: Wedges and Plate Bandes Mechanical Theories After De La Hire En L Architrave Le Plancher La Plate Forme Nouvelle Histoire De La Construction Pag 405 435 Presses Polytechniques Et Universitaires Romandes (2012). Wedges and plate-bandes: mechanical theories after de la hire
32. Huerta Fernández, S.: Mechanics of masonry vaults: The equilibrium approach (2001)
33. Huerta Fernández, S.: The use of simple models in the teaching of the essentials of masonry arch behaviour (2005)
34. Iannuzzo, A., Gesualdo, A., Olivieri, C., Montanino, A.: 3d exploration of internal stresses due to lateral loads and foundation movements in a semi-circular arch. In: COMPDYN Proceedings, pp. 2476–2491 (2023). https://www.scopus.com/inward/record.uri?eid=2-s2.0-85175847244&partnerID=40&md5=8edeef8ffd0b5e72961ce432ffed7a61
35. Itasca Consulting Group: 3DEC — Three-Dimensional Distinct Element Code, Version 7.0. Itasca Consulting Group, Minneapolis, Minnesota (2020). www.itascacg.com/software/3dec
36. Lemos, J.V.: Discrete element modeling of masonry structures. Int. J. Architectural Heritage **1**(2), 190–213 (2007). https://doi.org/10.1080/15583050601176868
37. Leseur, T.: Parere di tre mattematici sopra i danni, che si sono trovati nella cupola di San Pietro sul fine dell'anno 1742, Verlag nicht ermittelbar (1742)
38. Livesley, R.K.: Limit analysis of structures formed from rigid blocks. Int. J. Numer. Meth. Eng. **12**(12), 1853–1871 (1978)
39. Mascolo, I., Gesualdo, A., Olivieri, C., Fortunato, A.: On blocks detection in unilateral masonry-like structures: a rigid-elastic displacement approach. Int. J. Masonry Res. Innov. **7**(4), 395–405 (2022). https://doi.org/10.1504/IJMRI.2022.123750
40. McInerney, J., DeJong, M.: Discrete element modeling of groin vault displacement capacity. Int. J. Archit. Heritage **9**(8), 1037–1049 (2015). https://doi.org/10.1080/15583058.2014.923953
41. Montanino, A., De Gregorio, D., Olivieri, C., Iannuzzo, A.: The continuous airy-based for stress-singularities (cass) method: an energy-based numerical formulation for unilateral materials. Int. J. Solids Struct. **256**, 111954 (2022). https://doi.org/10.1016/j.ijsolstr.2022.111954
42. Montanino, A., Iannuzzo, A.: A quadrilateral plate-type finite element to model stress singularities in no-tension materials. Comput. Methods Appl. Mech. Eng. **432**, 117433 (2024). https://doi.org/10.1016/j.cma.2024.117433
43. Montanino, A., Olivieri, C., Zuccaro, G., Angelillo, M.: From stress to shape: equilibrium of cloister and cross vaults. Appl. Sci. **11**(9), 3846 (2021). https://doi.org/10.3390/app11093846
44. Mousavian, E., Bagi, K., Casapulla, C.: Interlocking joint shape optimization for structurally informed design of block assemblages. J. Comput. Des. Eng. **9**(4), 1279–1297 (2022). https://doi.org/10.1093/jcde/qwac054
45. Olivieri, C., Iannuzzo, A., Fortunato, A., DeJong, M.J.: The effect of concentrated loads on open-well masonry spiral stairs. Eng. Struct. **272**, 114952 (2022). https://doi.org/10.1016/j.engstruct.2022.114952

46. Paris, V., Gobbin, F., Nannei, V., Resmini, M., Mirabella Roberti, G.: Distinct element method analyses for damage assessment: the northern spur of valverde bulwark in the venetian fortress of bergamo. Int. J. Archit. Heritage **19**(5), 687–701 (2025). https://doi.org/10.1080/15583058.2024.2345701
47. Paris, V., Olivieri, C., Adriaenssens, S.: The impact of construction on the structural design of a complex masonry curved shell. Int. J. Space Struct. **40**(2–3), 180–194 (2025). https://doi.org/10.1177/09560599251381901. All Open Access, Hybrid Gold Open Access
48. Pingaro, N., Buzzetti, M., Gandolfi, A.: A numerical strategy to assess the stability of curved masonry structures using a simple nonlinear truss model. Buildings **15**(13), 2226 (2025). https://doi.org/10.3390/buildings15132226
49. Pingaro, N., Cardani, G., Coronelli, D., Milani, G.: On the stability of masonry arches through limit analysis and a nonlinear finite element-based method. In: International Conference on Protection of Historical Constructions, pp. 201–208. Springer (2025). https://doi.org/10.1007/978-3-031-87316-4_25
50. Pingaro, N., Milani, G.: Simple interface element equipped with thickness for the non-linear static heterogeneous analysis of masonry walls in-plane loaded: Implementation and validation. Eng. Struct. **351**, 122056 (2026). https://doi.org/10.1016/j.engstruct.2025.122056
51. Pingaro, N., Milani, G., Tiberti, S.: Automatic cad kinematic limit analysis approach for the limit analysis of masonry towers. In: AIP Conference Proceedings, vol. 2293, p. 380006. AIP Publishing LLC (2020). https://doi.org/10.1063/5.0026420
52. Poleni, G., Poleni, J.: Memorie Istoriche Della Gran Cvpola Del Tempio Vaticano, E De'Danni Di Essa, E De'Ristoramenti Loro, Divise In Libri Cinqve. Nella Stamperia del seminario (1748)
53. Portioli, F., Casapulla, C., Gilbert, M., Cascini, L.: Limit analysis of 3d masonry block structures with non-associative frictional joints using cone programming. Comput. Struct. **143**, 108–121 (2014). https://doi.org/10.1016/j.compstruc.2014.07.010
54. Pourfouladi, M., Pingaro, N., Valente, M.: Polibrick plugin as a parametric tool for digital stereotomy modelling. Comput. Struct. **311**, 107722 (2025). https://doi.org/10.1016/j.compstruc.2025.107722
55. Roberti, G.M., Ruscica, G., Paris, V.: From the herringbone dome by sangallo to the serlio floor of emy (and beyond). Curved Layered Struct. **8**(1), 259–270 (2021). https://doi.org/10.1515/cls-2021-0023
56. Sinopoli, A., Aita, D., Foce, F.: Further remarks on the collapse of masonry arches with coulomb friction. In: Proceedings of the 5th International Conference on Arch Bridges, pp. 649–657 (2007)
57. Tempesta, G., Galassi, S.: Safety evaluation of masonry arches. a numerical procedure based on the thrust line closest to the geometrical axis. Int. J. Mech. Sci. **155**, 206–221 (2019). https://doi.org/10.1016/j.ijmecsci.2019.02.036
58. Trentadue, F., De Tommasi, D., Marasciuolo, N., Vitucci, G.: Thrust in a symmetric masonry arch with frictional joints on spreading supports. Acta Mech. **235**(2), 659–670 (2024). https://doi.org/10.1007/s00707-023-03759-0
59. Young, T.: A course of lectures on natural philosophy and the mechanical arts: in two volumes, vol. 2, Johnson (1807)